Influence of Stark Broadening on Ion Temperature Measurement for ITER Divertor Diagnosis*)

Motoshi GOTO[1,2), Kunpei NOJIRI[3)], Joseph John SIMONS[2)], Tomoko KAWATE[1,2)], Tetsutarou OISHI[4)], Eiichi YATSUKA[3)], Yuto YANAGIHARA[1)], Mitsutaka ISOBE[1,2)] and Yoshihiko NUNOYA[3)]

[1)]*National Institute for Fusion Science, Toki 509-5292, Japan*
[2)]*Graduate University for Advanced Studies, SOKENDAI, Toki 509-5292, Japan*
[3)]*Naka Institute for Fusion Science and Technology, National Institutes for Quantum Science and Technology, Naka 311-0193, Japan*
[4)]*Department of Quantum Science and Energy Engineering, Tohoku University, Sendai 980-8579, Japan*

(Received 21 August 2024 / Accepted 16 October 2024)

The Stark broadening of a Be II line ($1s^2 3d\,^2D - 1s^2 4f\,^2F$, 467.339 nm) under a magnetic field is evaluated with the divertor plasma of ITER in mind. The electron and ion perturbers are treated in the impact and static approximations, respectively. The perturbation term due to the magnetic field is included in the static approximation. The results show that the Stark broadening comes to be significantly large when the density is higher than 10^{21} m^{-3}, and the ion temperature would be overestimated if the Stark broadening is not taken into account.

Keywords: ITER divertor, ion temperature measurement, beryllium, impurity line, Stark broadening, Zeeman effect

DOI: 10.1585/pfr.20.2401012

1. Introduction

The divertor impurity monitor diagnostics of ITER [1], the so-called DIM, consists of several UV-visible spectrometers, and is responsible for measuring emission lines of impurity ions in the divertor region, and the measured data will be utilized for the plasma control, device protection, physical research, and so on.

Because a beryllium- or other low Z material-coating is considered for the divertor and the first wall plates in the current ITER design baseline, those impurity atoms are expected to be introduced into the divertor plasma. On the other hand, since the requirements for DIM include the ion temperature (T_i) measurement, the use of emission lines of these impurity ions may be considered. More specifically, DIM is supposed to use the Doppler broadening of those beryllium ion lines for the measurement of T_i.

Regarding beryllium ions, some Be II and Be III lines are expected to have high emissivities in the UV-visible wavelength range based on the results of SOLPS-ITER [2], which is a plasma boundary code package based on the plasma and neutral transport codes, i.e., B2.5 [3] and EIRENE [4], respectively.

For accurate T_i measurements, it is necessary to consider other effects on the emission line profile besides Doppler broadening. Firstly, there is an effect caused by magnetic fields. The magnetic field strength in ITER plasma is typically 5 T, and so emission lines would split into some components due to the Zeeman effect. The splitting width depends on the field strength and on the quantum state regarding the angular momentum of the upper and lower levels of the transition. When the splitting width is comparable to the Doppler broadening width, the Zeeman effect could contribute to the observable broadening width.

Secondly, the SOLPS-ITER calculation indicates the electron density of the divertor plasma could exceed 10^{21} m^{-3} near the target plates [5] where T_i is a few eV or lower. In such high density conditions, it is possible that the Stark broadening also influences the evaluation of the broadening width for the T_i measurement. We here attempt to calculate the Stark broadening for a Be II line ($1s^2 3d\,^2D - 1s^2 4f\,^2F$, 467.339 nm) with a fixed magnetic field of 5 T and quantitatively evaluate their influence on the T_i measurement. This line was chosen because of the structure of the upper and lower energy levels, which was expected to be highly affected by the Stark broadening.

It is noted that we focus on an emission line of the beryllium ion in this paper, but it is highly likely that ITER will not use beryllium. Even so, the method used in this study is universal and can be applied to any other ions without any difficulty.

2. Calculation Method

We adopt the same calculation method used in Ref. [6]

author's e-mail: goto.motoshi@nifs.ac.jp

*) This article is based on the presentation at the 26th International Conference on Spectral Line Shapes (ICSLS2024).

for the Stark broadening, i.e., ion and electron contributions are treated as the static and impact approximations, respectively, and the convolution of these profiles is regarded as the observable line profile.

For the impact approximation, the data found in Ref. [7] are adopted, where the line profile is approximated by the Lorentz function and is represented by the full width at half maximum (FWHM). The width is assumed to be proportional to the perturbers density, and its proportionality coefficient is given for respective lines. The FWHM for the present Be II line is approximated by $0.508\times(n_e/10^{23})$ nm, where n_e is the electron density and in m^{-3}. The electron temperature is assumed to be 1000 K [7].

For the static approximation, a distribution function of the electric field strength as a collection of microfields created by ions is considered. The Holtsmark distribution [8] is used for the present calculation. The perturbers are dominated by protons and its density is assumed to be equal to that of electrons. We assume an isotropic plasma so that the resulting electric field distribution is also isotropic. The difference from the condition in Ref. [6] is that there exists a magnetic field which is oriented in a specific direction and makes the system axisymmetric with respect to the magnetic field.

We calculate the emission line profile in the presence of an electric field $\boldsymbol{E}$ of a certain direction and strength, together with a fixed magnetic field $\boldsymbol{B}$, and superpose the line profiles by scanning the strength and direction of the electric field to obtain the line profile to be observed.

The Hamiltonian H under a magnetic field and an electric field can be written as

$$H = H_0 - \boldsymbol{\mu}\cdot\boldsymbol{B} - \boldsymbol{E}\cdot\boldsymbol{d}, \tag{1}$$

where H_0 is the non-perturbed Hamiltonian, $\boldsymbol{\mu}$ is the magnetic moment of the atom, and $\boldsymbol{d}$ is the electric-dipole moment. When we take the quantization axis $\boldsymbol{z}$ in the direction of $\boldsymbol{B}$, and denote the direction of $\boldsymbol{E}$ as $\boldsymbol{\xi}$, Eq. (1) can be rewritten as

$$H = H_0 - \mu_B B(g_L L_z + g_S S_z) - E d_\xi, \tag{2}$$

where $B = |\boldsymbol{B}|$, $E = |\boldsymbol{E}|$, μ_B is the Bohr magneton, $g_L\,(=1)$ and $g_S\,(\approx 2)$ are the orbital and spin g-factors, respectively, L_z and S_z are the z-axis components of the orbital and spin angular momentum quantum numbers, and d_ξ is the ξ direction component of $\boldsymbol{d}$.

The first term gives diagonal elements of H which correspond to the level energies without perturbation fields, and the matrix elements due to the second term are obtained by the conventional method to deal with the Zeeman effect [9].

For evaluating the matrix elements due to the electric field perturbation, i.e., $\langle LJM| - Ed_\xi|L'J'M'\rangle$,we first rewrite the eigenstates $|LJM\rangle$ in the coordinates with the quantization axis in the ξ direction. Such an operation can be made by the coordinates rotation [9] denoted by R, which turns the z-axis in the $\boldsymbol{E}$ or the ξ-axis direction.

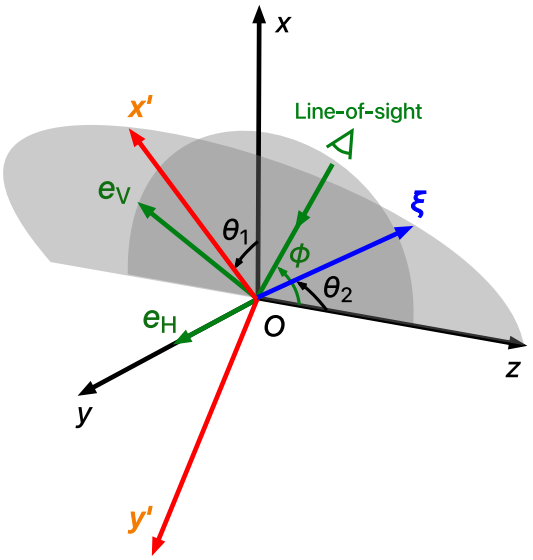

Fig. 1 Euler rotation for turning the quantization axis (z-axis) into the ξ-axis direction by first rotating θ_1 around the z-axis and then θ_2 around the y'-axis which is the new y-axis after the first rotation. The definition of observation vectors $\boldsymbol{e}_H$ and $\boldsymbol{e}_V$ are also shown: The former is in the x-z plane and is perpendicular to the line-of-sight, and the latter is on the y-axis.

Following the Euler rotation formalism, the rotation R can be realized by first rotating θ_1 around the z-axis and then θ_2 around the new y-axis, i.e., y'-axis in Fig. 1. The resulting state $|LJM\rangle_\xi$ can be expressed as

$$|LJM\rangle_\xi = D(R)|LJM\rangle, \tag{3}$$

where $D(R)$ is the operator for the rotation R. With the use of the inverse operator $D(R^{-1})$, Eq. (3) can be rewritten as

$$|LJM\rangle = D(R^{-1})|LJM\rangle_\xi \tag{4}$$

$$= \sum_m |LJm\rangle_\xi D^{(J)}_{mM}(R^{-1}) \tag{5}$$

$$= \sum_m |LJm\rangle_\xi D^{(J)*}_{Mm}(R), \tag{6}$$

where $D^{(J)}_{mM}(R^{-1})$ expresses the matrix elements of $D(R^{-1})$ for the case when the total angular momentum quantum number is J and is called the Wigner function. The last line is derived with the relation of $D^{(J)}_{mM}(R^{-1}) = D^{(J)*}_{Mm}(R)$ [10]. Matrix elements of the third term in Eq. (2) can be then rewritten as

$$\langle LJM| - Ed_\xi|L'J'M'\rangle \tag{7}$$

$$= -E\sum_{m,m'} D^{(J)}_{Mm}(R)D^{(J')*}_{M'm'}(R)\langle LJm|_\xi d_\xi|L'J'm'\rangle_\xi \tag{8}$$

$$= -E\sum_{m,m'} D^{(J)}_{Mm}(R)D^{(J')*}_{M'm'}(R)\langle LJm|d|L'J'm'\rangle, \tag{9}$$

where the self-evident relation

$$\langle LJm|_\xi d_\xi|L'J'm'\rangle_\xi = \langle LJm|d|L'J'm'\rangle, \tag{10}$$

is used.

Now all the matrix elements are obtained and we can calculate the perturbed energy levels by diagonalizing Eq. (2). In general, the degeneracy is resolved and the magnetic sublevels come to have different energy values. Each eigenstate is obtained as a linear combination of unperturbed states where the coefficients correspond to the eigenvector elements derived in the diagonalization of Eq. (2).

Such calculations are performed for the upper and lower states of the transition, and the wavelengths of the resolved line components are obtained as the differences between the upper and lower level energies.

Next, the intensity of each line component is considered. The line intensity is proportional to the square of the electric dipole moment corresponding to the upper and lower state combination. By giving the wavelengths and intensities for respective lines, the entire spectrum is synthesized as a sum of all the line components.

In this calculation, we must be aware that the observable line intensities depend on the angle between the line-of-sight and the magnetic and/or electric field because each resolved line component is polarized. We assume that the line-of-sight is in the x-z plane and has an angle ϕ with z-axis as shown in Fig. 1. The observable line intensity is obtained as a sum of two linearly polarized components which are perpendicular to each other.

The basis vectors corresponding to the direction of the two linear polarization components are here called the observation vectors. One observation vector is chosen so as to be parallel to the y-axis, and the other is in the x-z plane and perpendicular to the line-of-sight as shown in Fig. 1. The former and latter observation vectors are denoted $\boldsymbol{e}_{\mathrm{H}}$ and $\boldsymbol{e}_{\mathrm{V}}$, respectively.

The line intensity of a transition from $|u\rangle$ to $|l\rangle$ states is here represented by the square of the matrix component of the corresponding electric dipole moment as

$$I = |\langle l|\boldsymbol{e}\cdot\boldsymbol{d}|u\rangle|^2, \tag{11}$$

where $\boldsymbol{e}$ stands for $\boldsymbol{e}_{\mathrm{H}}$ or $\boldsymbol{e}_{\mathrm{V}}$, and $\boldsymbol{d}$ is the electric dipole moment. Their scalar product $\boldsymbol{e}\cdot\boldsymbol{d}$ can be expanded in the spherical coordinates as

$$\boldsymbol{e}\cdot\boldsymbol{d} = -e_1 d_{-1} + e_0 d_0 - e_{-1} d_1. \tag{12}$$

The coefficients $e_{\pm1}$ and e_0 can be expressed as

$$e_0 = \gamma, \tag{13}$$

$$e_{\pm1} = \mp\frac{1}{\sqrt{2}}(\alpha \pm \mathrm{i}\beta), \tag{14}$$

where α, β, and γ are the x-, y-, and z-axis components of the observation vector $\boldsymbol{e}$. In the present case, $\alpha = \gamma = 0$, and $\beta = 1$ for $\boldsymbol{e}_{\mathrm{H}}$ and $\alpha = \cos\phi$, $\beta = 0$, and $\gamma = \sin\phi$ for $\boldsymbol{e}_{\mathrm{V}}$. We here assume to observe the plasma from an upper port with a line-of-sight looking down on the divertor at an angle of 30 degrees from the vertical to the toroidal direction, i.e., ϕ is approximately 60 degrees. In the following calculations we will use this value for ϕ.

Evaluation of Eq. (11) requires the spherical components of the electric dipole moment

$$\langle l|d_q|u\rangle, \tag{15}$$

with $q = 0, \pm1$. As derived above, an eigenstate under external field perturbations is understood to be a linear combination of unperturbed states. Here, $|l\rangle$ and $|u\rangle$ can be expressed by unperturbed lower state $|l'_r\rangle$ and upper state $|u'_s\rangle$ as

$$|l\rangle = \sum_r C^l_r |l'_r\rangle, \tag{16}$$

$$|u\rangle = \sum_s C^u_s |u'_s\rangle, \tag{17}$$

where C^l_r and C^u_s are the elements of the eigenvectors obtained by the diagonalization of Eq. (2). The term $\langle l|d_q|u\rangle$ is then rewritten as

$$\langle l|d_q|u\rangle = \sum_{r,s} C^l_r C^u_s \langle l'_r|d_q|u'_s\rangle. \tag{18}$$

Now we write the basis states $|l'_r\rangle$ and $|u'_s\rangle$ explicitly as

$$|l'_r\rangle = |L_1 J_1 M_1\rangle, \tag{19}$$

$$|u'_s\rangle = |L_2 J_2 M_2\rangle. \tag{20}$$

In this case, with a help of the Wigner-Eckart theorem and the Racah algebra, each component in Eq. (18) can be written as [11]

$$\begin{aligned}\langle l'_r|d_q|u'_s\rangle &= \langle L_1 J_1 M_1|d_q|L_2 J_2 M_2\rangle \\ &= (-1)^{(J_1 - M_1)+(S+1+L_1+J_2)}\sqrt{(2J_1+1)(2J_2+1)} \\ &\times \begin{pmatrix} J_1 & 1 & J_2 \\ -M_1 & q & M_2 \end{pmatrix} \begin{Bmatrix} L_1 & J_1 & S \\ J_2 & L_2 & 1 \end{Bmatrix} \langle L_1\|d\|L_2\rangle,\end{aligned} \tag{21}$$

where $(\cdots)$ and $\{\cdots\}$ are the 3-j and 6-j symbols, respectively. The last factor in Eq. (21), which is called the reduced matrix element, is related to the line strength S' as

$$\langle L_1\|d\|L_2\rangle = \pm\alpha_0\sqrt{\frac{S'}{2S+1}}, \tag{22}$$

where a_0 is the Bohr radius and S' is in the atomic units. The positive and negative signs correspond to the cases $L_1 = L_2 + 1$ and $L_1 = L_2 - 1$, respectively. Equation (11) can be now evaluated, and each line component for a given combination of $\boldsymbol{B}$, $\boldsymbol{E}$, and $\boldsymbol{e}$ is obtained.

By performing such calculations for all combinations of magnetic sublevels in the upper and lower levels, and for $\boldsymbol{e}_{\mathrm{H}}$ and $\boldsymbol{e}_{\mathrm{V}}$, the intensities of all observable emission line components are obtained for a given combination of $\boldsymbol{B}$ and $\boldsymbol{E}$. For evaluation of the Stark broadening, a weighted integral following the Holtsmark distribution should be performed with respect to the electric field strength. Furthermore, since the electric field can be oriented in any direction, integration over all directions must be also performed.

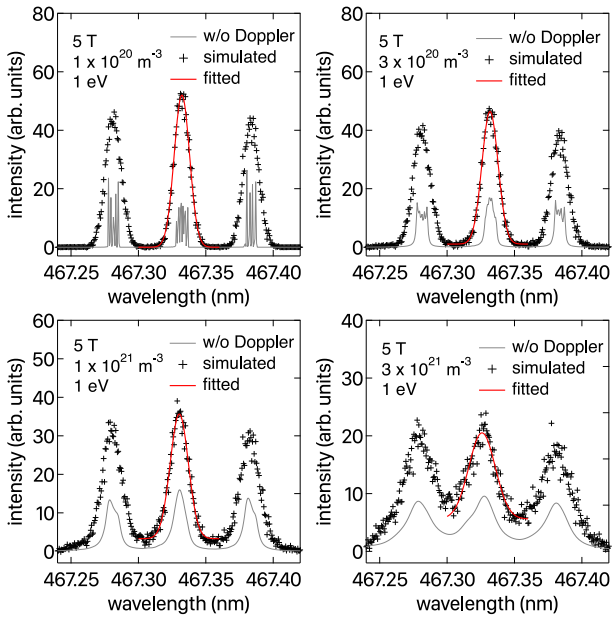

Fig. 2 Examples of calculated spectra of the Be II line ($1s^2 3d\ ^2D - 1s^2 4f\ ^2F$, 467.339 nm) for four different perturber density cases when T_i = 1 eV.

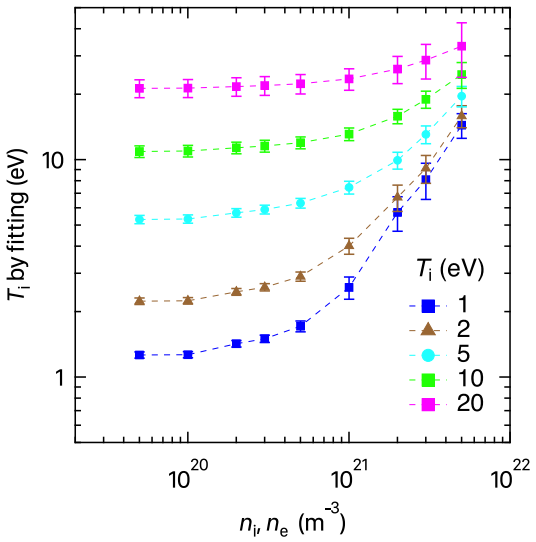

Fig. 3 Density dependence of T_i derived via fitting of calculated spectrum with a single Gaussian function.

It is noted that if the perturbation is only the electric field, the difference in the observable intensity of the polarization component due to the direction of the electric field relative to the line-of-sight is averaged out, so it is not necessary to integrate for the electric field direction and simply take the sum of emission intensities of the π and σ lights. However, because isotropy cannot be assumed due to the presence of a fixed magnetic field, it is necessary to integrate for all directions for the electric field.

Finally, the obtained spectrum is convoluted with the impact approximation broadening and the desired emission line profile with the Stark broadening in a magnetic field is obtained.

3. Results and Discussion

Figure 2 shows the spectra calculated for some different perturber density values. The thin lines show the spectra calculated with the method discussed in the previous section. The cross symbols show the convolution of the spectra with the Doppler broadening of 1 eV. Here, we give each data point a random error following the Poison distribution considering that fitting will be later performed with the Gaussian function to derive T_i.

It can been seen that the line is divided into three main peaks. The central peak and the two lateral peaks correspond to the π and σ components of the Zeeman split line, respectively. The intensity ratio of the π and σ components is mainly determined by the angle between the line-of-sight and the magnetic field, which is about 60 degrees.

Assuming a simple T_i measurement, the central peak is fitted with a single Gaussian, and T_i is determined from its width. Figure 3 shows the results for cases of T_i = 1, 2, 5, 10, and 20 eV. It is readily noticed that the evaluated T_i increases with the density especially in the range where the density is higher than 10^{21} m^{-3}. This is considered to be an effect of the Stark broadening. The error is evaluated as the root mean square of the difference between the measured and the fitted data. It is also seen that the obtained temperature error increases with increasing density because the shape of the emission lines is no longer well represented by a single Gaussian.

It should be noted that even when the density is lower than 10^{20} m^{-3}, T_i obtained by fitting is higher than the assumed temperature value. This is caused by the splittings of emission line components due to the Zeeman effect.

In summary, we have studied the Stark broadening in a magnetic field for a beryllium ion emission line. When the electron density exceeds 10^{21} m^{-3}, which is a possible condition in the ITER divertor plasma, it has been confirmed that the Stark broadening becomes significant so that the ion temperature measurement can be affected.

Acknowledgments

This work was performed partially under the support of the NIFS Collaboration Research Program (NIFS22KIEH003). M.G. thanks Nader Sadeghi for discussions on the calculation method. M.G. also thanks Annette Calisti for her helpful suggestions.

[1] https://www.iter.org/
[2] E. Kaveeva *et al.*, Nucl. Mater. Energy **35**, 101424 (2023).
[3] V. Kotov *et al.*, Juel-Report, 4257 (2007).
[4] D. Reiter *et al.*, Fusion Sci. Technol. **47**, 172 (2005).
[5] R.A. Pitts *et al.*, Nucl. Mater. Energy **20**, 100696 (2019).
[6] N. Sadeghi and M. Goto, J. Quant. Spectrosc. Radiat. Transf. **245**, 106875 (2020).

[7] H.R. Griem, Spectral line broadening by plasmas, Academic Press, New York (1974).
[8] C.F. Hooper, Phys. Rev. **169**, 193 (1968).
[9] T. Fujimoto and A. Iwamae, Plasma Polarization Spectroscopy, Springer, Berlin (2007).
[10] J.J. Sakurai, Modern Quantum Mechanics, Addison-Wesley, Redwood City (1985).
[11] P.H. Heckmann and E. Träbert, Introduction to the Spectroscopy of Atoms, North-Holland, Amsterdam (1989).